Acta Astronautica 219 (2024) 41–47

Contents lists available at ScienceDirect

Acta Astronautica

journal homepage: www.elsevier.com/locate/actaastro

Investigation of aluminium Whipple Shield response to hypervelocity impacts close to ballistic limit between 2.5 and 5 km/s

Lorenzo Olivieri [a,*], Rannveig Marie Faergestad [b], Cinzia Giacomuzzo [a], Stefano Lopresti [a], Giovanni Pitacco [c], Alessandro Francesconi [d], Tiziana Cardone [e], Jens Kristian Holmen [f], Tore Borvik [b]

[a] CISAS "G. Colombo", University of Padova, Via Venezia 15, 35131, Padova, Italy
[b] SIMLab, Department of Structural Engineering, NTNU – Norwegian University of Science and Technology, Richard Birkelands Veg 1a, 7491, Trondheim, Norway
[c] University of Padova, Via VIII Febbraio 2, 35122, Padova, Italy
[d] DII-CISAS - University of Padova, Via Venezia 15, 35131, Padova, Italy
[e] European Space Agency (ESA), the Netherlands
[f] Enodo AS, NO-3044, Drammen, Norway

ARTICLE INFO

Keywords:
Space debris
Whipple shield
Hypervelocity impact

ABSTRACT

For impact velocities larger than a threshold velocity of 3 km/s, aluminium Whipple Shields present an enhanced protection capability with respect to monolithic protections with the same areal density. In particular, in the range between 3 and 7 km/s the projectile partially fragments and melts after impacting the bumper; modelling this transition might be complex due to the high number of parameters affecting the collision. In particular, limited data is available in literature with a systematic evaluation of such parameters.

In this context, a campaign of 22 experiments was performed to assess the response of aluminium Whipple Shields to normal impacts of aluminium projectiles in the transition range up to 5 km/s. In the tests, the projectile diameter was fixed at 2.9 mm and the bumper thickness and impact velocity were systematically varied respectively at 1, 1.5, and 2 mm and between 2.6 and 5 km/s. Collected data included high-velocity videos of the debris cloud generated by the impacts at both low resolution (for all shots) and high resolution (for 19 out of 22 tests); in addition, for 10 experiments high-resolution images of both the bumper and the wall were acquired after the tests.

In this paper, the experimental campaign is described and the main collected results are presented; in particular, the influence of the different impact parameters is discussed. Experimental results are finally compared with numerical simulations conducted with a smoothed particle hydrodynamics method available in IMPETUS Solver.

1. Introduction

Whipple Shields were originally conceived to protect spacecraft vessels from meteoroids impacts [1]; once the issue of human-made debris was finally recognized [2], their utilization on crewed vehicles was better investigated [3]. To date, more efficient or less bulky protection are often employed on spacecraft; however, Whipple Shields are often employed as reference when comparing the ballistic properties of different protections [4,5] or developing new Ballistic Limit Equations (BLEs) [6,7].

In their first and simplest configuration, Whipple Shields consist of two-wall structures separated by a stand-off distance. Due to this geometry, Whipple Shields present an enhanced protection capability with respect to monolithic structures with the same areal density: the first wall, commonly referred as bumper, can partially fragment or melt an impacting projectile, creating an internal debris cloud that could be less dangerous for the rear wall compared to a single, massive impactor.

The ballistic response of a Whipple Shield is directly related to the impact velocity [3]. For low velocities (ballistic regime, below

* Corresponding author.
E-mail addresses: lorenzo.olivieri@unipd.it (L. Olivieri), rannveig.m.fargestad@ntnu.no (R.M. Faergestad), cinzia.giacomuzzo@unipd.it (C. Giacomuzzo), stefano.lopresti@unipd.it (S. Lopresti), giovanni.pitacco.1@gmail.com (G. Pitacco), alessandro.francesconi@unipd.it (A. Francesconi), tiziana.cardone@esa.int (T. Cardone), jens@enodo.no (J.K. Holmen), tore.borvik@ntnu.no (T. Borvik).

https://doi.org/10.1016/j.actaastro.2024.03.009
Received 25 November 2023; Received in revised form 18 January 2024; Accepted 6 March 2024
Available online 7 March 2024

Nomenclature

c	Velocity of sound in the material, km/s
d_b	Diameter of bumper hole, mm
d_p	Projectile diameter, mm
m	Mass, g
S_1	Stand-off length, mm
S_{WP}	Distance rear wall – witness plate, mm
t_b	Bumper thickness, mm
t_w	Wall thickness, mm
v	Impact velocity, km/s
ρ	Density, kg/m^3

approximately 3 km/s for aluminium plates) the shield behaves similarly to a monolithic plate with equivalent thickness, as the projectile mostly remains intact after impact with the bumper. For high velocities (hypervelocity regime, above approximately 7 km/s for aluminium), the bumper fully fragments and/or melts the projectile, generating a cloud of small fragments that act as a distributed pressure wave on the rear plate; in this regime, the Whipple Shield has its best performance with respect to a monolithic plate. In the intermediate range (shatter regime), the projectile fragmentation is only partial and generates a mixed debris cloud, with a residual central large fragment; the rear wall is therefore subjected both to a distributed load from the small debris in the cloud and a localised impact from the largest fragment. This last regime is the most complex to model and represents a transition between ballistic and hypervelocity impacts; in BLEs, it is usually represented by a linear interpolation between the limits of the two other regimes [8].

The development of Whipple Shields BLE required expensive and complex ground experiments; for this reason, data available in literature is often limited to punctual experiments, with no parametric investigation on the many parameters that may affect shield perforation, such as walls thickness on projectile diameter ratio, stand-off size, material, and impact velocity. A few exceptions are the experiments on aluminium plates from Piekutowski (impact velocities between 3.77 and 7.38 km/s, ratio $t_b/d_p = 0.049$, i.e. a projectile significantly larger than the thickness of the bumper, [9]), Chi (impact velocities between 3.16 and 5.17 km/s, ratio t_b/d_p of 0.157 and 0.210, [10]), and Wen (impact velocities between 2.2 and 5.2 km/s, t_b/d_p ratios from 0.078 to 0.315, [11]). In a similar fashion, only limited information is available on the debris clouds generated by the bumper and expanding in the stand-off.

With the objective to better comprehend the transition between ballistic and shatter regime and the effect of the main parameters affecting it, a campaign of impact tests was conceived and recently performed through a collaboration between Delft University of Technology, Norwegian University of Science and Technology, and University of Padova. In the tests, the plate material, the rear wall thickness, the stand-off distance, and the projectile diameter were fixed and only the bumper thickness and impact velocity were systematically varied, to obtain a full set of data and understand the effect of those parameters on the Whipple Shield. The experimental data also included videos of the debris cloud generated by the bumper from high-speed cameras, to better identify the transition from a large central fragment to a more distributed debris cloud. Experimental results are currently being analysed [12] and will be employed for the development and validation of numerical codes under investigation by the involved institutions [13,14].

This paper presents a summary of the experimental campaign and a selection of the main results. Next section describes the test facility and setup and describes the performed experiments. Section 3 compares the experimental results with the Whipple Shield analytical BLEs developed by Christiansen [3]. Section 4 summarized the preliminary analysis of the bumper plates and the high-velocity videos. Section 5 finally compares a selection of test data with numerical simulations conducted with a coupled finite element-discrete element method available in LS-DYNA.

2. Experimental campaign

The experimental campaign was performed with the Light Gas Gun (LGG) in the hypervelocity impact test laboratory of the University of Padova [15,16]. The current facility can be seen in Fig. 1; it is capable of accelerating projectiles up to 100 mg at a maximum speed of 5.5 km/s and with a high shot frequency, up to 10 experiments per day, achievable due to a specific setup which employs reusable components in the whole main gas gun subsystem [17,18].

The experimental setup can be seen in Fig. 2 (left) and consisted in a Whipple Shield configuration, with the addition of a Witness plate behind the rear wall. All plates were in Aluminium AA6061-T6, with a 20 × 20 cm^2 area; both the witness plate and the rear wall had a thickness of 3 mm, while three bumper thicknesses (1, 1.5, and 2 mm) were considered in the campaign. The plates were mounted with elastic springs to a movable frame (Fig. 2, right), allowing fast target preparation and recovery from the LGG impact chamber.

Two high velocity cameras, a Phantom v2511 and a Phantom M310, were employed to capture the development of the debris cloud. They were placed outside the LGG impact chamber, in line with the midpoint between the bumper and the rear wall; the fields of view of the two cameras were placed on orthogonal planes to reconstruct the cloud shape in three dimensions (see Fig. 3).

In the tests, the projectile diameter was fixed at 2.9 mm and the bumper thickness and impact velocity were systematically varied respectively at 1, 1.5, and 2 mm and at 2.60, 3.00, 3.30, 4.00, 4.65, and 5.00 km/s. The experimental campaign consisted of 22 shots, listed in Table 1. In three experiments, only the Phantom M310 camera was able to record the impact (CAMERA label in the table notes); in other nine tests the target was contaminated by sabot failures (SABOT label in the table notes), but it was still possible to detect the debris cloud

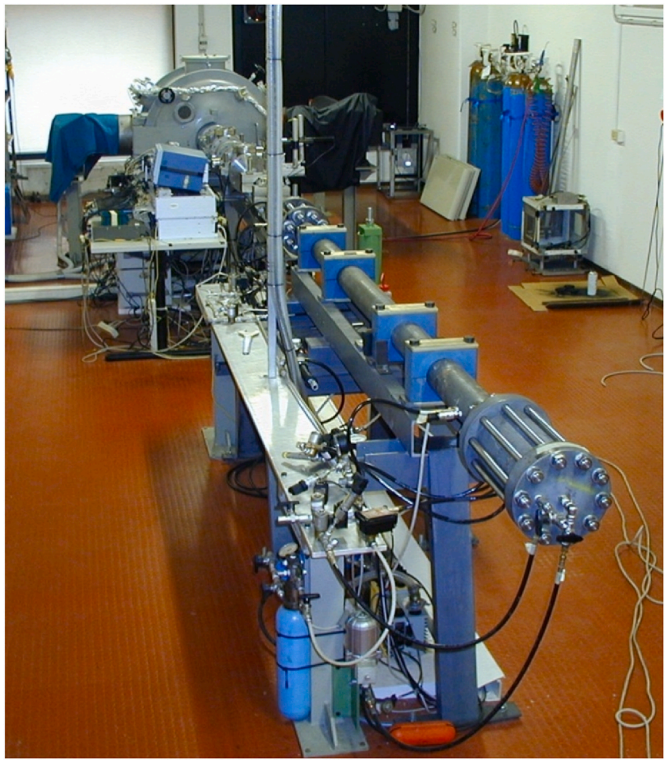

Fig. 1. Cisas hypervelocity impact facility with the light gas gun.

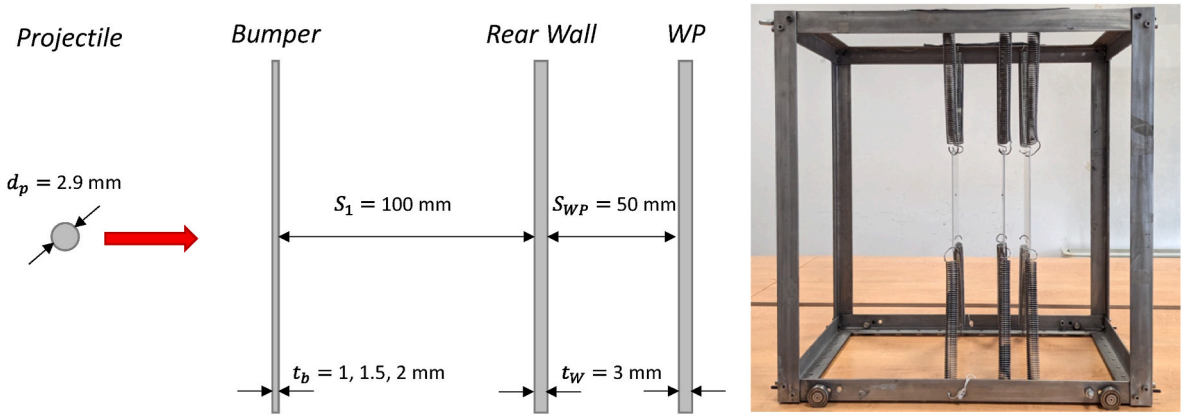

Fig. 2. Test configuration with Whipple Shield and Witness Plate (left) and experimental setup mounted on a suspension system (right).

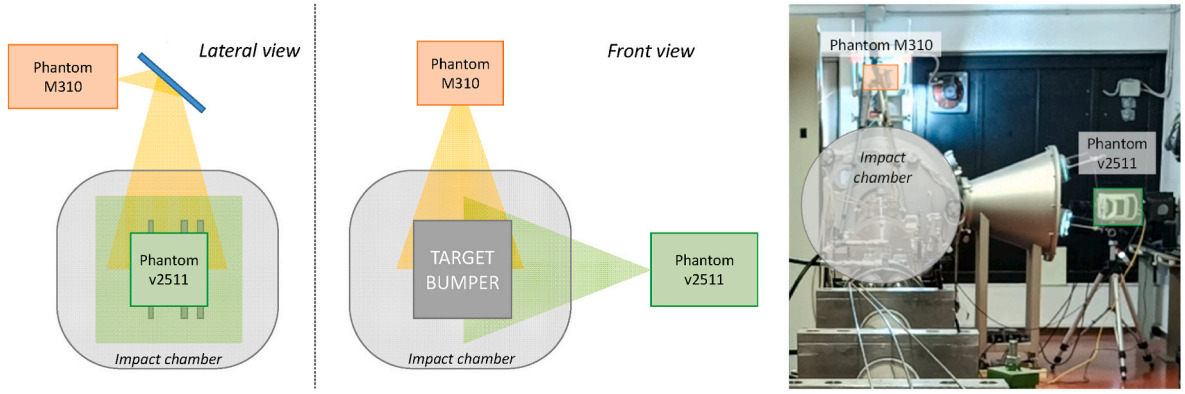

Fig. 3. On the left: high-velocity cameras configuration and fields of view (not in scale). On the right, the two cameras placed on top and on the side of the impact chamber.

Table 1
Summary of the experimental campaign. The labels CAMERA and SABOT in the notes of a test indicate respectively that only the Phantom M310 was able to record the impact or that the sabot contaminated on the target. For tests #9244, #9249, #9258, and #9260 the red letter P indicates the failure of the rear wall.

Nominal velocity, km/s	Plate thickness								
	1 mm			1.5 mm			2 mm		
	vel, km/s	SHOT #	NOTES	vel, km/s	SHOT #	NOTES	vel, km/s	SHOT #	NOTES
2.60	2.60	9265	/	2.59	9263	/	2.62	9266	/
				2.64	9264	/			
3.00	3.12	9254	SABOT	3.05	9261	SABOT	/	/	/
3.30	3.36	9247	CAMERA	3.27	9248	/	3.22	9253	/
							3.28	9249	P, CAMERA
4.00	3.99	9246	/	3.96	9244	P	3.99	9245	/
	4.02	9243	CAMERA						
4.65	4.63	9252	SABOT	4.65	9250	/	4.71	9251	SABOT
5.00	4.97	9260	P, SABOT	4.95	9255	SABOT	4.85	9256	SABOT
	5.00	9258	P, SABOT				4.93	9259	SABOT

perforation diameter on the bumper.

Fig. 4 shows the debris cloud (top) and the damages on bumper and rear wall (bottom) for test #9244, with bumper thickness of 1.5 mm and impact velocity of 3.96 km/s. The perforation of the bumper generated a large cloud, with a dense front. The damage on the rear wall consisted in surface craterisation and deposit. On the rear wall back face a detached spall was detected, indicating the failure of this shield.

In the reminder of this paper, the failure of a shield (due to detached spall, e.g. shot #9244, or perforation, e.g. #9249, of the rear wall) will be indicated by P; shields passing this failure criterion will be indicated as NP.

3. Ballistic limit investigation

Among the 22 performed tests, only four (the aforementioned #9244 and shots #9249, #9258, and #9260) led to the failure of the rear wall; for experiments #9258 and #9260, this was due to the contamination from the sabot. The failure mode for tests #9244 (t_b = 1.5 mm, v = 3.96 km/s) and #9249 (t_b = 2.0 mm, v = 3.28 km/s) can be seen in Fig. 6 (left and centre) and can be classified as detached spall, indicating that for these impact conditions the Whipple Shield is slightly above its ballistic limit. It can be noted that for the latter case, a similar test (#9253, t_b = 2.0 mm, v = 3.22 km/s, Fig. 6 on the right) was classified as NP, suggesting that the ballistic limit is not a rigid threshold but should be at

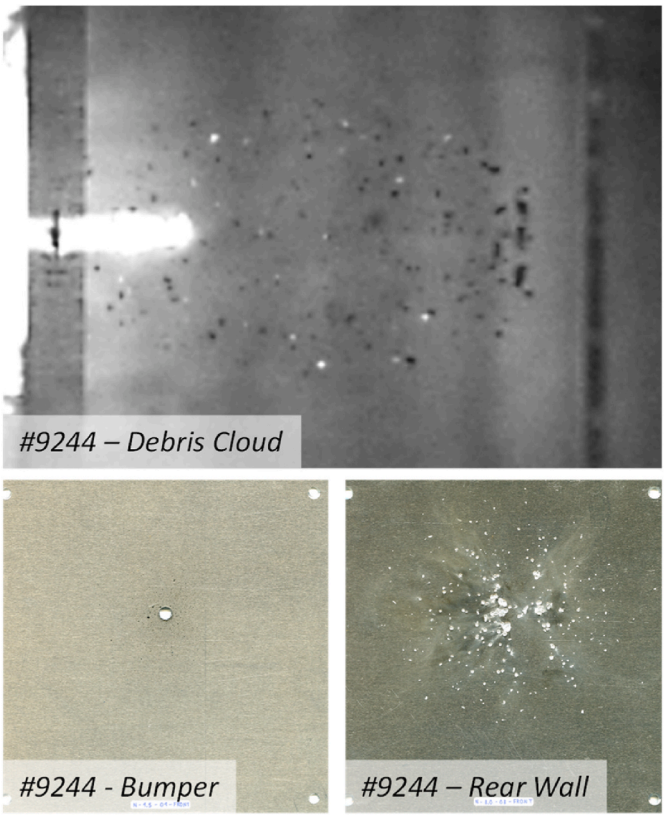

Fig. 4. Shot #9244 (t_b = 1.5 mm, v = 3.96 km/s, failure due to spalling). On top, debris cloud generated by the bumper. On bottom, damage on bumper front plate (left) and rear wall (right).

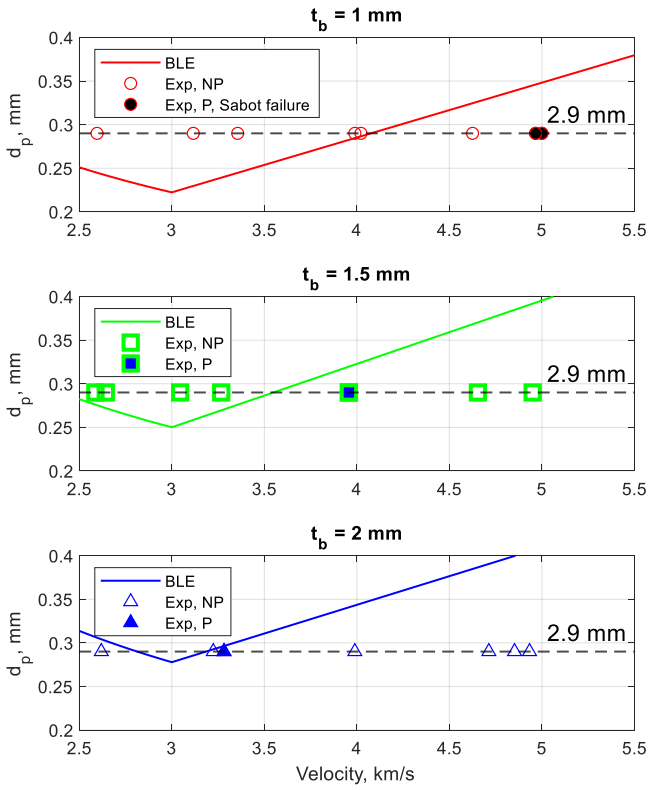

Fig. 5. BLEs and experiments data for the three bumper thicknesses. NP – Not Perforated, P – Perforated.

least expressed within an uncertainty band; this approach would be in accordance with the models developed in Ref. [19].

This can be better appreciated in Fig. 5, in which the experiments are compared with the BLEs developed by Christiansen [3], i.e. the curve indicating the limit between the Whipple Shield failure (P, area above the curve) and survivability (NP, below the BLE). It can be observed that for t_b = 1 mm (top), the BLE predicts perforation for velocities below approximately 4 km/s; however, all the valid tests (i.e. not considering #9268 and #9260, with sabot failure) did not perforate the Whipple Shield. This suggests that for this bumper thickness the BLE underestimates the shield performance. With respect to the intermediate thickness (t_b = 1.5 mm, centre), it can be noted another deviation from BLE prediction: the two lower velocity tests, above the BLE, did not perforate the shield, but for test #9244, below the BLE, a detached spall indicated the failure of this configuration. Last, for t_b = 2 mm the two tests in close proximity to the BLE (# 9249 and #9253) resulted in a failure (P) and a non-perforation (NP). These preliminary results further suggest that the transition between ballistic and shatter regimes should be better investigated, in order to obtain more reliable BLEs that may consider different failure causes or transition thresholds (e.g. Ref. [20]).

4. Test data analysis

In this section, the first results of this experimental campaign are presented; the samples are still under analysis and additional results might be obtained in the future.

It shall be underlined that due to the different sabot contaminations the experiments reported in Table 1 could be only partially employed in the following analysis. With respect to the investigation of the bumper hole (section 4.1), in addition to all successful experiments for a large section of the sabot contaminations the sabot impact point was different from the projectile one, allowing the identification of the hole; for this reason, only shots #9251, #9254, #9258, #9259, and #9260 were discharged. On the contrary, for the investigation of the mass lost from the bumper (section 4.2) all sabot failures could not be used. Last, for debris cloud parameters reconstruction (section 4.3) the sabot contaminated experiments were still employable in the analysis, as in the interval between projectile and sabot impact on the bumper it was possible to record at least a few frames of the debris cloud expansion.

4.1. Bumper hole diameter

For the impact parameters selected in this campaign, the bumper can be considered a thin plate; the t_b/d_p ratios are between 0.34 and 0.69. In all successful tests it was possible to measure the diameter of the perforation hole on the bumper; this was valid also for a subset of the experiments with sabot failure: in these experiments, high-speed videos showed that the sabot fragments collided with the bumper after projectile perforation and the determination of the projectile hole was still possible.

Fig. 7 compares the measured bumper hole diameter with the predictions for thin plates from Hill [21]; the analytical equations are reported in Appendix A. It can be observed that for the thinnest bumper (1 mm, red triangles and lines) experimental data and models are in accordance (average difference below 0.1 mm). On the contrary, a larger deviation can be observed for the 2-mm thick bumper, in particular for the lowest velocities: at 2.62 km/s the difference between prediction and measurement is of about 0.77 mm on a 5.5 mm diameter. However, the prediction error in this case is still below 15%, suggesting that the Hill's equations can still represent the order of magnitude of the bumper perforation hole.

4.2. Mass lost from bumper

Before and after each impact test, the bumper plates were weighed

Fig. 6. Rear wall back face damages for shots #9244 (t_b = 1.5 mm, v = 3.96 km/s, P), #9249 (t_b = 2.0 mm, v = 3.28 km/s, P), and #9253 (t_b = 2.0 mm, v = 3.22 km/s, NP).

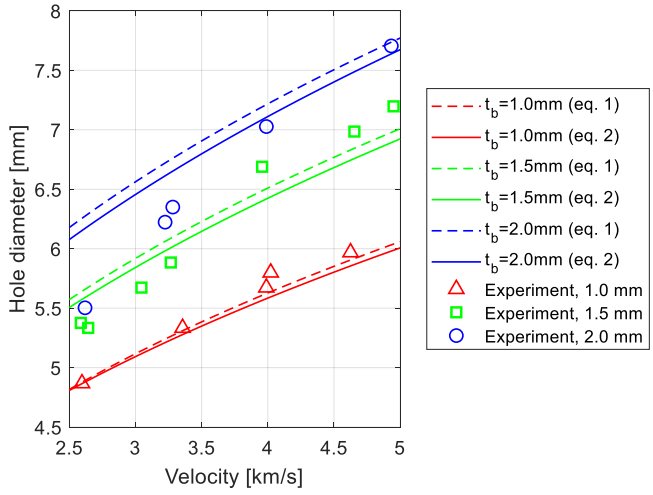

Fig. 7. Comparison of measured bumper perforation holes with the analytical models from Hill [18].

with a scale with 0.001 g resolution. This allowed evaluating the amount of mass lost by the bumper due to the impact. In this analysis, experiments with sabot contamination were discharged.

Fig. 8 shows the lost mass for the successful experiments. As expected, thicker plates are more affected by the impact, as the projectile can interact with a larger fraction of material before perforating the bumper. Results from the thinner (red triangles) and the thicker (blue circles) configurations show a quasi-linear trend with the velocity and a strong influence of the thickness. The 1.5 mm thick plate data is scattered between the other values, but present a strongly non-linear trend; in particular, the test at 3.27 km/s, #9248, shows a lost mass on the bumper comparable to the 2-mm thick plate, that would need further investigation.

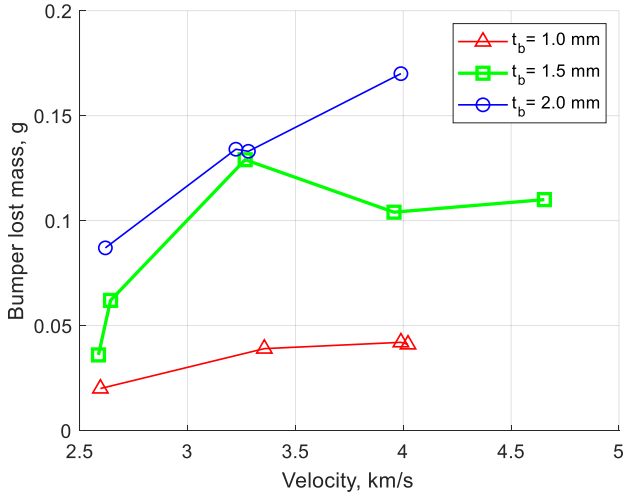

Fig. 8. Mass lost by the bumper due to the impact.

4.3. Debris cloud parameters

The debris clouds that developed between the bumper and the rear wall were captured using the high-speed cameras, and features of the clouds were measured in each frame. The main measurement points are shown in Fig. 9. A parameter l_c is defined, measuring the distance between the rear side of the bumper and the front fragment of the debris cloud. The maximum debris cloud diameter d_c is then measured for each frame and corresponding l_c. To compare the debris cloud measurements, all tests were evaluated at $l_c \approx 90$ mm, right before the debris cloud impacts the rear wall.

Fig. 10 shows the debris cloud diameter d_c as a function of the bumper thickness t_b for the test series at 2.6. km/s and 5 km/s. The debris cloud diameter is larger for higher impact velocities, and is found to decrease with increasing bumper thickness. For the test series at 5 km/s, the decrease is linear, and for the test series at 2.6 km/s, the results flatten out after 1.5 mm bumper thickness.

The residual velocity v_{res} of the debris cloud is measured as the average velocity of the front fragment from all frames over the length l_c, and is shown in Fig. 11 as a function of the bumper thickness t_b for the test series at 2.6. km/s and 5 km/s. The residual velocity, shown in the figure as a percentage of the impact velocity v, is higher for higher impact velocities, and decreases with increasing bumper thickness. For the 2 mm bumper thickness, the velocity is reduced by an equal

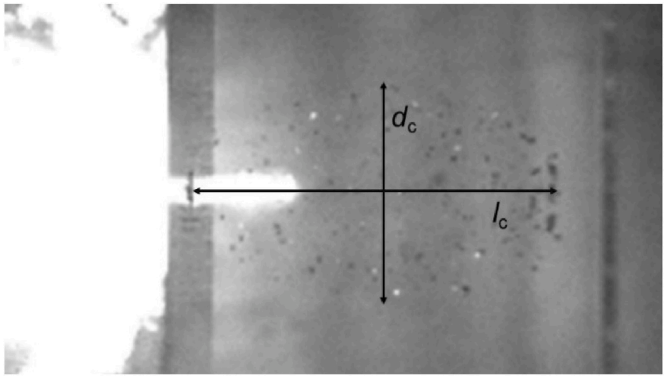

Fig. 9. Measurement points of debris clouds.

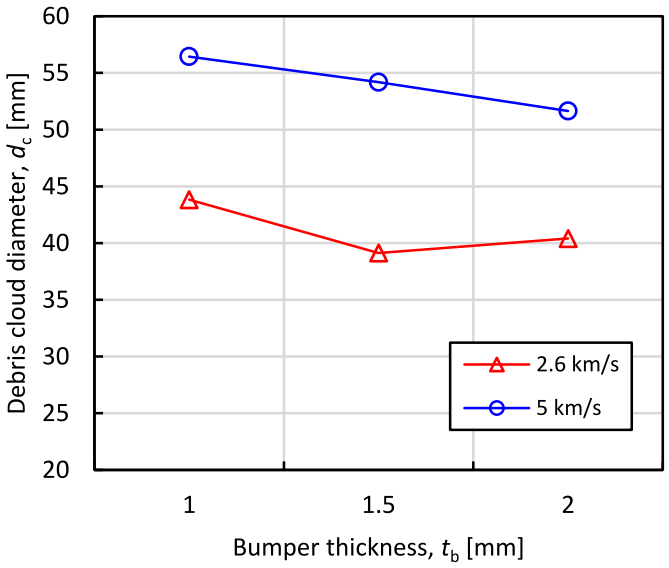

Fig. 10. Debris cloud diameter d_c as a function of the bumper thickness t_b, measured at $l_c = 90$ mm.

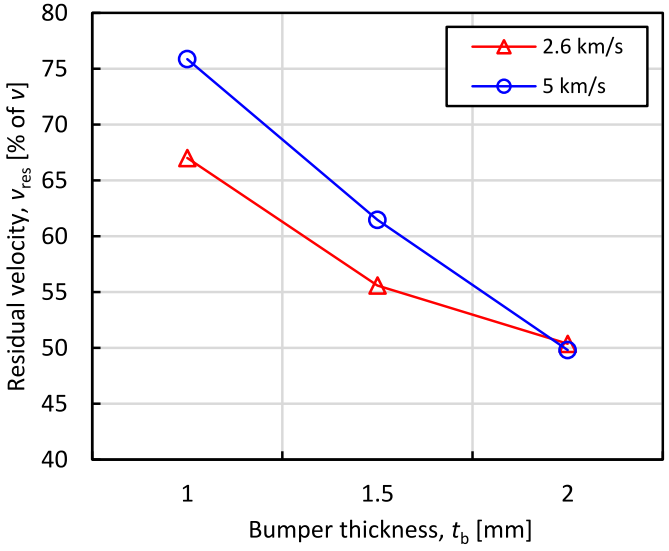

Fig. 11. Residual velocity V_{res} as a function of the bumper thickness t_b.

percentage for 2.5 and 5 km/s.

5. Comparison with numerical simulations

Numerical models of the Whipple shield configurations were established in IMPETUS Solver using an SPH (smoothed particle hydrodynamics) formulation. This solver is developed by IMPETUS Afea to predict large deformations of structures and components exposed to extreme loading conditions, such as explosions, blasts, and impacts. For this model, the modified Johnson-Cook constitutive relation [22,23] is applied, combined with the Mie-Grüneisen equation of state (EOS). The material data for these models for Aluminium 6061-T6 are adapted from Færgestad et al. [13], where a full description of the models can also be found. The models were set up with a total of approximately 30 million SPH particles, and a bumper of reduced size (2×2 cm^2) to limit the computational time, as shown in Fig. 12.

The numerical results for one configuration (#9250) are shown in Figs. 13 and 14, compared to the corresponding experimental results. First, the debris clouds are compared at $l_c \approx 90$ mm in Fig. 13, right

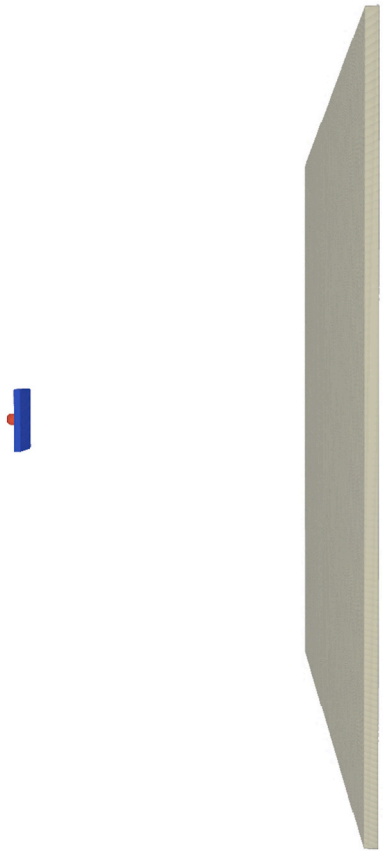

Fig. 12. Numerical model of Whipple shield configuration.

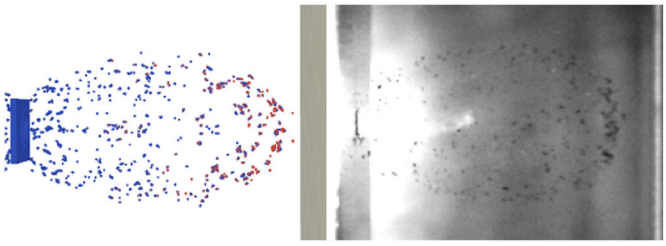

Fig. 13. Comparison between numerical simulation and experimental result for the debris cloud at $l_c \approx 90$ mm in test #9250. The bumper material in the simulation is shown in blue, and the projectile material is shown in red. (For interpretation of the references to colour in this figure legend, the reader is referred to the Web version of this article.)

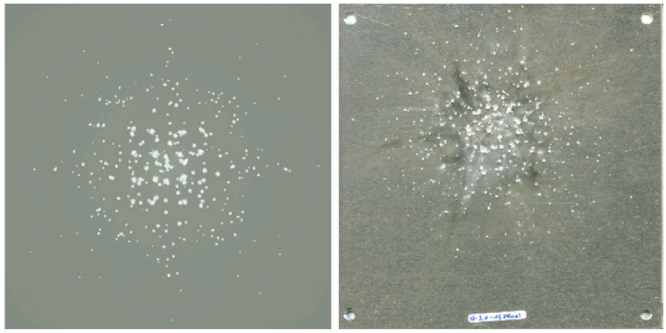

Fig. 14. Comparison between numerical simulation and experimental result for the damage pattern on the rear wall in test #9250.

before the debris cloud impacts the rear wall. Then, the damage pattern created by the debris cloud on the rear wall is compared in Fig. 14. For the damage pattern visualisation, a temperature contour plot of the rear wall is used, where SPH particles with increased temperature as a result of impact are white, while the unaffected particles are grey. There is generally good agreement between the numerical and experimental results. The debris cloud is somewhat narrower in the numerical simulation than in the experiments, but the overall shape and distribution of fragments is similar. The damage pattern on the rear wall is similar in both size and shape, and the craters are of similar size and distribution.

6. Conclusions

In this work a campaign of experimental tests on a Whipple Shield configuration was presented. 22 experiments were executed, fixing the projectile diameter at 2.9 mm and systematically varying the bumper thickness at 1, 1.5, and 2 mm and the impact velocity between 2.6 and 5 km/s. Only three tests showed the failure of the Whipple Shield, mainly due to spalling phenomena; the comparison with Christiansen's BLE suggest that the transition between ballistic and shatter regimes should be better investigated with further experiments.

Data analysis showed accordance between measurements of the hole diameter in the first plate and prediction from literature models; in addition, the main parameters of the debris cloud propagating inside the Whipple Shield were obtained.

Last, the comparison of experimental data with numerical simulations performed with IMPETUS Solver showed good accordance in terms of the reconstruction of the debris cloud and the damage pattern on the rear wall.

Declaration of competing interest

The authors declare that they have no known competing financial interests or personal relationships that could have appeared to influence the work reported in this paper.

Acknowledgments

This work has been partially supported by the Centre of Advanced Structural Analysis (CASA), Centre for Research-based Innovation, at the Norwegian University of Science and Technology (NTNU) and the Research Council of Norway through project no. 237885 (CASA). The authors wish to thank ESA for supplying the target materials for the study and IMPETUS Solver for support with the numerical simulations.

Appendix A. Hill damage equations

The following damage equations, developed by Hill [21], were employed to predict the bumper hole diameter. Subscripts p and t indicates respectively the projectile and the target (that is, in this case, the bumper).

Eq. (1):

$$d_h = 3.309\, d_p \left(\frac{V}{c_p}\right)^{0.033} \left(\frac{V}{c_t}\right)^{0.298} \left(\frac{\rho_p}{\rho_t}\right)^{0.022} \left(\frac{t_t}{d_p}\right)^{0.359}$$

Eq. (2):

$$d_h = 2.947\, d_p \left(\frac{V}{c_p}\right)^{0.055} \left(\frac{V}{c_t}\right)^{0.339} \left(\frac{\rho_p}{\rho_t}\right)^{0.028} \left(\frac{t_t}{d_p}\right)^{0.414} + 0.342\, d_p$$

References

[1] F.L. Whipple, Meteorites and space travel, Astron. J. 52 (1947) 131.
[2] D.J. Kessler, B.G. Cour-Palais, Collision frequency of artificial satellites: the creation of a debris belt, J. Geophys. Res.: Space Phys. 83 (A6) (1978) 2637–2646.
[3] E.L. Christiansen, Design and performance equations for advanced meteoroid and debris shields, Int. J. Impact Eng. 14 (1–4) (1993) 145–156.
[4] E.L. Christiansen, et al., Enhanced meteoroid and orbital debris shielding, Int. J. Impact Eng. 17 (1995) 217–228, 1-3.
[5] L. Olivieri, et al., Experimental characterization of multi-layer 3D-printed shields for microsatellites, J. Space Saf. Eng. 7 (2) (2020) 125–136.
[6] A. Francesconi, et al., An engineering model to describe fragments clouds propagating inside spacecraft in consequence of space debris impact on sandwich panel structures, Acta Astronaut. 116 (2015) 222–228.
[7] S. Ryan, F. Schaefer, R. Destefanis, M. Lambert, A ballistic limit equation for hypervelocity impacts on composite honeycomb sandwich panel satellite structures, Adv. Space Res. 41 (7) (2008) 1152–1166.
[8] Eric L. Christiansen, et al., Handbook for designing MMOD protection. NASA Johnson Space Center, 2009. *NASA/TM-2009-214785*.
[9] A.J. Piekutowski, Formation and Description of Debris Clouds Produced by Hypervelocity Impact, 1996.
[10] R.Q. Chi, B.J. Pang, G.S. Guan, Z.Q. Yang, Y. Zhu, M.J. He, Analysis of debris clouds produced by impact of aluminum spheres with aluminum sheets, Int. J. Impact Eng. 35 (12) (2008) 1465–1472.
[11] K. Wen, X.W. Chen, R.Q. Chi, Y.G. Lu, Analysis on the fragmentation pattern of sphere hypervelocity impacting on thin plate, Int. J. Impact Eng. 146 (April) (2020) 103721.
[12] R.M. Færgestad, et al., Experimental study of hypervelocity impact against aluminium Whipple Shields, in: Proceedings 17th ECSSMET, 28 - 30 March 2023. Toulouse, France.
[13] R.M. Færgestad, et al., Coupled finite element-discrete element method (FEM/DEM) for modelling hypervelocity impacts, Acta Astronaut. 203 (2023) 296–307.
[14] A. Francesconi, et al., Numerical simulations of hypervelocity collisions scenarios against a large satellite, J. Impact Eng. 162 (2022) 104130.
[15] L. Olivieri, C. Giacomuzzo, S. Lopresti, A. Francesconi, Research at the university of Padova in the field of space debris impacts against satellites: an overview of activities in the last 10 years, Appl. Sci. 13 (6) (2023) 3874.
[16] D. Pavarin, A. Francesconi, Improvement of the CISAS high-shot-frequency light-gas gun, Int. J. Impact Eng. 29 (2003) 549–562.
[17] F. Angrilli, D. Pavarin, M. De Cecco, A. Francesconi, Impact facility based upon high frequency two-stage light-gas gun, Acta Astronaut. 53 (2003) 185–189.
[18] A. Francesconi, D. Pavarin, A. Bettella, F. Angrilli, A special design condition to increase the performance of two-stage light-gas guns, Int. J. Impact Eng. 35 (2008) 1510–1515.
[19] S. Ryan, et al., Artificial neural networks for characterising Whipple shield performance, Int. J. Impact Eng. 56 (2013) 61–70, 2013.
[20] S. Ryan, et al., Whipple shield performance in the shatter regime, Int. J. Impact Eng. 38 (6) (2011) 504–510.
[21] S.A. Hill, Determination of an empirical model for the prediction of penetration hole diameter in thin plates from hypervelocity impact, Int. J. Impact Eng. 30 (3) (2004) 303–321.
[22] G.R. Johnson, W.H. Cook, A constitutive model and data for metals subjected to large strains, high strain rates and high temperatures, Proc. 7th Int. Symposium on Ballistics (1983) 541–547.
[23] T. Børvik, O.S. Hopperstad, T. Berstad, M. Langseth, A computational model of viscoplasticity and ductile damage for impact and penetration, Eur. J. Mech. Solid. 20 (5) (2001) 685–712.